



1

2 Summer-time episodic chlorophyll-a blooms near east coast of Korea

3

4 Young-Tae Son, Jae-Hyoung Park, and SungHyun Nam^{*}

5 Seoul National University, Seoul, Republic of Korea

6

7 ^{*}Correspondence to namsh@snu.ac.kr

8

9

10

11



12

13 **Abstract**

14 We present intensive observational data of surface chlorophyll-a bloom episodes occurring over
15 several days in the summers of 2011, 2012, and 2013, accompanying the equatorward advection
16 of low sea-surface salinity (SSS) water near the east coast of Korea. Time-series analysis of
17 meteorological and oceanographic (physical and biochemical) parameter data, such as chlorophyll
18 fluorescence (CF) from surface mooring, ocean color (chlorophyll a and total suspended sediment),
19 sea surface height (satellite-derived), and serial hydrographic data (from in-situ measurements)
20 were used to investigate the relationship between surface bloom events and changes in seawater
21 characteristics and currents. In the summers of the three years, a total of 10 bloom events (E01–
22 E10) were identified where the surface CF was significantly ($> 2 \mu\text{g/l}$) enhanced over a relatively
23 long (> 1 day) period. The bloom events in the summers of 2011 and 2012 accompanied low or
24 decreasing SSS for several days to a week after heavy rainfalls at upstream stations and
25 equatorward currents. Unlike the typical 8 of the 10 events (80 %), E07 was potentially derived
26 from the onshore advection of high CF offshore water of southern origin into the coastal zone near
27 the mooring, whereas E10 is likely prevailed by offshore advection of high CF plume water trapped
28 by the coastal area. Contrasting with many coastal systems, these findings indicate that event-scale
29 productivity near the east coast of Korea in summer is not controlled by local blooms triggered by
30 either nutrients or light availability, but by the equatorward and cross-shore advectons of high CF
31 plume water.

32

33

34

35



36 **1. Introduction**

37 Biological blooms associated with, among others, the horizontal advection of chlorophyll-rich water (often
38 having low-salinity and high nutrients linked to heavy rain, e.g., nutrient loading), have been frequently
39 observed in many coastal systems (e.g. Yin et al., 2004; Dai et al., 2008; Halverson and Pawlowicz, 2013;
40 Reifel et al., 2013). Blooms stimulated by plume-delivering nutrients and enhanced stratification were
41 observed near and offshore of Hong Kong (Dai et al., 2008; Yin et al., 2004). During bloom events, a several-
42 fold increase in chlorophyll a (Chl a) and significant shift in phytoplankton community structure were
43 observed (Dai et al., 2008). The effects of effluent discharge plume on coastal phytoplankton communities
44 were examined from the City of Los Angeles Hyperion Wastewater Treatment Plant, demonstrating localized
45 blooms occurred a few days after the diversion within the effluent plume (Reifel et al., 2013). The Fraser
46 River plume affects Chl a distribution in the Strait of Georgia, British Columbia, Canada, revealing large
47 differences with respect to the plume, despite insensitivity in the long-term average (Halverson and
48 Pawlowicz, 2013).

49 There are several small river plumes potentially affecting Chl a distribution near and offshore of the east
50 coast of Korea; yet, the effects remain poorly understood. High summer (from June to September, JJAS)
51 precipitation often accompanying heavy rainfall around the Korean peninsula is well known and accounts
52 for more than 50% of the annual precipitation in the region. During summer, most rivers in the region become
53 flooded and discharge large volumes of freshwater into the adjacent marginal seas, including the East Sea
54 (Japan Sea), Yellow Sea, and East China Sea (Bae et al., 2008; Kong et al., 2013). Chl a distribution in the
55 southwestern East Sea off the east coast of Korea has been examined, and found to be associated with
56 physical processes at mesoscale or larger scales, including spring and fall blooms that have been detected
57 using satellite ocean color data, data from limited short-duration ship surveys (Hyun et al., 2008; Kang et al.,
58 2004), and time-series data collected continuously from moored buoys (Hong et al., 2013; Son et al., 2014).
59 Despite wide range images available from geostationary and polar-orbit satellite ocean color remote sensing
60 (Yoo and Kim, 2004; Son et al., 2014; Hyun et al., 2008; Kim et al., 2011), phytoplankton blooms observed
61 over several days to weeks near the coast, particularly during the well-stratified summer season, have rarely
62 been examined. Thus, we aimed to address the episodic bloom events in summer and investigate the effects
63 of river plumes on Chl a distribution near and away from the east coast of Korea.

64

65 **2. Data and methods**

66 Time-series data of meteorological, physical, and biochemical parameters have been measured using a
67 surface mooring named ESROB (East Sea Real-time monitoring Ocean Buoy), deployed in water at 130 m
68 depth, about 8 km off the mid-east coast of Korea (Fig. 1). The data collected includes wind speed and
69 direction at 2 m above the sea surface, photosynthetically active radiation (PAR) at about 2 m above the sea
70 surface and at 10 m depth, temperature and salinity at five depths (5 m, 20 m, 40 m, 60 m, and 110 m), vertical
71 profile of current with an interval (bin size) of 4 m (upper most bin corresponds to 5 m depth), and sea surface



72 temperature (SST), salinity (SSS), dissolved oxygen (DO), and chlorophyll fluorescence (CF) measured by
73 a Water Quality Monitor (WQM) at about 1 m depth. Details on the technical design, improvements, and
74 early-phase operations of ESROB have been previously described (Nam et al., 2005). In the present study,
75 we used data collected for ~ 3 years, from April, 2011 to December, 2013, with an emphasis on the three
76 summer periods (JJAS) when the alongshore current averaged over 6 years reversed to an equatorward
77 direction (Park et al., 2016).

78 The CF as a factory-calibrated Chl a concentration in units of $\mu\text{g/l}$ following the manufacturer's (WET
79 Lab) instructions is needed to calibrate with in-situ measurements owing to long-term sensor drift. Four
80 cruises were conducted in July and October 2011, April 2012, and July 2013 to collect in-situ water samples
81 for Chl a and in-situ sensor measurements for water temperature and salinity near the coast. A statistically
82 significant correlation ($r^2 = 0.76$, $p < 0.001$) was found between the CF sensor values and in-situ chlorophyll
83 concentration derived from the spectrophotometer using acetone-extracted Chl a (Fig. 2a). In addition to the
84 chlorophyll calibration, the concentrations of nitrate were analyzed simultaneously with 64 samples to
85 determine the nitrate proxy based on the relationship between temperature and nitrate. Separately, to observe
86 the fine-scale coastal SST and SSS distributions around the ESROB, in-situ measurements using a small
87 research vessel equipped with a thermosalinograph (SEB21, 10 s sampling interval) were conducted on July
88 30, 2013, a couple of days after heavy rainfall. Since non-photochemical quenching (NPQ) has a significant
89 influence on the CF in response to changes in ambient light (Müller et al., 2001), particularly for a single
90 channel excitation Chl a fluorometer, the effects were corrected from the ESROB CF data following the
91 methods described in Halverson and Pawlowicz (2013) before calibrating with in-situ water samples.

92 We used high-resolution daily data generated by the geostationary ocean color satellite (composited using
93 eight images) to estimate surface Chl a distributions. The spatial resolution of the geostationary satellite is
94 500 m at a grid 50 times further than previous polar orbiting ocean color satellites (Ryu et al., 2012). Chl a
95 concentration observed from the ocean color satellite can be easily contaminated by the total suspended
96 sediment (TSS) and colored dissolved organic matter (CDOM) in the coastal regions (Ryu et al., 2012). Thus,
97 the satellite-measured Chl a was calculated through software modules applying a correction algorithm for
98 the TSS and CDOM, as well as by minimizing the contaminating effects of cloud, sea fog, and aerosols (level
99 1B). Nevertheless, relationships between the satellite-measured Chl a and TSS in coastal and offshore areas
100 in Fig. 1 were compared with a linear regression to determine the Chl a in the coastal region (Fig. 2b, c).
101 Results exhibited that the higher the value, the wider the scatter. This indicated that Chl a can be measured
102 regardless of the TSS both in the coastal and outer sea, which supports the possibility of using the satellite-
103 derived Chl a in this area. Satellite altimeter-derived sea surface height (SSH) products corrected using
104 coastal tide-gauge sea level data along the east coast of Korea (Choi et al., 2012) were used to examine
105 surface geostrophic currents around and offshore of the ESROB in the summer of 2013. Precipitation data
106 were also used to compare the bloom timings with those of heavy rainfalls in summer. Precipitation in unit
107 of mm/day recorded every 3 hours at stations during the summers of 2011, 2012, and 2013 along the coast
108 (SP: SinPho, HH: HamHeung, WS: WonSan, JJ: JangJun, SO: Sockcho, BGN: BukGangNeung, DH:
109 DongHae) were proxied as freshwater discharges from several small rivers into the East Sea (Fig. 1).



110 Current and wind vectors were corrected for local magnetic deviation, decomposed into alongshore and
111 cross-shore components rotating counter-clockwise from the north by 30 degrees. Wind stresses have been
112 calculated following $\vec{\tau} = \rho_a C_D |W| \vec{W}$ (ρ_a : air density, C_D : drag coefficient, \vec{W} : wind), and alongshore and
113 cross-shore components of current (V_a and U_c) and wind stress (WS_a and WS_c) are expressed by the
114 coordinate transformation, respectively (Large and Pond, 1981). All variables were low-pass filtered with
115 the half power centered at 40 h.

116

117 3. Results

118 3.1. Climatological CF variations

119 Annual cycles of wind stress (WS_a , WS_c), surface CF, SST, SSS, surface DO, and surface current ((V_a , U_c)
120 at the upper most bin) observed at the ESROB were obtained by climatologically averaging monthly mean
121 values over the three years from 2011 to 2013, which showed significant summer-time CF enhancements (in
122 addition to two well-documented blooms in spring and fall), weakened wind forcing, increased SST,
123 decreased SSS, over-saturated surface DO (though absolute DO decreased), and strengthened equatorward
124 ($V_a < 0$) surface currents (Fig. 3). The enhancements of CF during the summer with significantly high
125 concentrations over 1 $\mu\text{g/l}$ in July accompanied with decreased SSS (abruptly decreased from June to July)
126 and strengthened equatorward currents (maximum speed of 15 cm/s in July), implied high Chl a and low
127 salinity water of northern origin. Although absolute DO decreased with increasing SST, the surface water
128 was over-saturated for most of the summer, implying a significant role of surface bioactivity. Weak poleward
129 ($V_a > 0$ and $U_a \sim 0$) surface currents were observed throughout the year, except in summer, when strong
130 equatorward ($V_a < 0$ and $U_a \sim 0$) currents prevailed.

131

132 3.2. CF events observed in summers of 2011, 2012, and 2013

133 In the summers of 2011, 2012, and 2013, 10 bloom events (E01–E10) were identified where the surface
134 CF was significantly enhanced over considerable period (Fig. 4, Table 1). The CF bloom events were defined
135 as follows: the peak CF reached higher than 2.0 $\mu\text{g/l}$ and the duration when the CF $> 2.0 \mu\text{g/l}$ was longer than
136 1 day, when CF $> 1.0 \mu\text{g/l}$. The summer bloom event lasted for several days to weeks, which is shorter than
137 the typical duration of spring and fall blooms. Six events, three each year (E01–E03 and E04–E06), were
138 identified in the summers of 2011 and 2012, whereas four (E07–E10) occurred in 2013 (Fig. 4). The average
139 SST, SSS, and CF for the duration of each event are listed in Table 1.

140 During the CF events in the summer of 2011 (E01–E03), low SSS was observed at the ESROB several
141 days to a week after remarkable wind forcing and heavy rainfalls (maximum of 160 mm/day during E02) at
142 upstream stations, accompanying enhanced equatorward currents (Fig. 5a, c, e and f). Two typhoons (MAON
143 and MUIFA) yielding a maximum wind stress of 0.25 N/m² passed through the region during the CF bloom



144 events, inducing strong equatorward (before E01) and poleward (after E03) wind stresses (arrows labeled by
145 M1 and M2 in Fig. 5b). Interestingly, the equatorward (poleward) wind stress may strengthen equatorward
146 (poleward) and onshore (offshore) surface currents. Indeed, strong equatorward currents were observed up
147 to 2 days after the peak wind forcing immediately before E01, whereas the equatorward currents were
148 markedly weakened by the poleward wind stress immediately after E03 (Fig. 5b, f).

149 Similarly, the CF events in the summer of 2012 were also accompanied by low or decreasing SSS several
150 days to a week after heavy rainfalls at upstream stations and equatorward currents (Fig. 6a, c, e and f). Three
151 (KHANUN, BOLAVEN, and TENBIIN) among the four typhoons in the summer affected the surface CF,
152 SSS, and surface currents during the events. Since typhoon KHANUN drove poleward wind stress, strong
153 equatorward currents developed before E04 were weakened, and SSS increased to reduce the salinity
154 stratification and decrease surface CF during E04 (arrow labeled by K in Fig. 6b, c, e and f). After the typhoon
155 passed, the surface CF increased again along with re-enhancing equatorward currents, re-stratifying salinity,
156 and decreasing SSS during E05 (Fig. 6c, e and f). Two typhoons (BOLAVEN and TENBIIN) successively
157 passed the area and both poleward (equatorward) wind stress re-stratified (well-mixed) upper ocean
158 conditions during E06. The poleward wind stress imposed by the BOLAVEN induced well-mixed conditions
159 with high SSS, low SST, and strong poleward surface currents (arrow labeled by B in Fig. 6b, c, d and f).
160 However, the reversed wind stress imposed by the successive TENBIN resulted in decreasing SSS, increasing
161 SST, weakening the poleward surface current (strengthening equatorward surface current), and rapidly
162 increasing surface CF (peak exceeding 4.5 $\mu\text{g/l}$) (arrow labeled by T in Fig. 6b, c, d, e and f).

163 Contrasting to the CF bloom events in the summers of 2011 and 2012, two among the four events (E07
164 and E10) in the summer of 2013 did not accompany preceding heavy enough rainfall at the upstream stations
165 nor equatorward currents (Fig. 7a, f). Typical heavy rainfalls and enhanced equatorward surface currents
166 preceded low SSS and high surface CF during the other two events (E08 and E09) only (Fig. 7a, f). Unlikely
167 with typical events, the SSS remained high and SST temporally decreased (negative anomaly) during E07
168 (Fig. 7c and 7d), whereas relatively high SST and low SSS were observed during E10 (Fig. 7c, d). Contrasting
169 with those in the other two years, winds were mild and no typhoon passage was reported in the summer of
170 2013 (Fig. 7b).

171

172 **3.3. Surface CF distributions**

173 The equatorward advection of low salinity, chlorophyll-rich plume water into the ESROB area along the
174 coast was confirmed from a series of daily composite satellite-measured Chl a only when clear images
175 containing few clouds were available. One example presented here is from four images continuously
176 available from July 24 to 27, 2013, before E09 (Fig. 9a, b, c and d). A high surface CF zone in the northern
177 area (e.g. off the SP, HH, and WS, Fig. 1) was separated from that in the southern area (e.g. between the
178 coast and UI, Fig. 1) following the poleward current—the East Korea Warm Current (EKWC)—and
179 extended equatorward with time near the coast during the period (Fig. 9a, b, c and d) after the heavy rainfalls



180 in July 19–24 (Fig. 7a). The high CF plume water was elongated and reached to JJ by July 24, SO by July
181 25–26, and farther south near the coast by July 27, yielding the E09 event from July 28 to August 1 (Table
182 1, Fig. 7). The SST and SSS observed using the thermosalinograph on July 30, 2013 in the vicinity of ESROB
183 consistently demonstrated wedge-shaped patterns with low SSS and high SST water confined near the coast
184 and reaching farther south passing BGN (Fig. 9e and 9f), confirming the equatorward advection of low-
185 salinity and high CF surface water along the coast to ESROB. Interestingly, the satellite-based surface
186 geostrophic currents around and offshore of the ESROB (not shown) and the alongshore currents observed
187 at the upper depths of the ESROB (e.g. Fig. 7f) were all equatorward during this period.

188 A pattern of surface CF distribution and geostrophic flow field on July 3, 2013 for E07 are shown in Fig.
189 9a and 9b, where high CF was found inshore of the poleward flowing EKWC (main axis is closer to UI than
190 the high CF area) and within cyclonic circulation around the ESROB (area of relatively low SSH). Onshore
191 currents prevailed between BGN and DH, associated with the cyclonic circulation (Fig. 9b), potentially
192 yielding onshore advection of high CF offshore water of southern origin into the coastal zone near the
193 ESROB during E07 (Fig. 9d). Similarly, although clear images were not available at that time, the
194 geostrophic flow field on August 21, 2013 for E10 is shown in Fig. 9c, wherein offshore currents were found
195 to prevail near the coastal zone. The offshore advection of coastal plume water of northern origin presumably
196 having low salinity, high temperature, and high CF (as cases of many other events, see Fig. 1 or Fig. 8) may
197 have enhanced the surface CF at the ESROB during E10 (Fig. 9e).

198

199 **4. Discussion**

200 **4.1. Horizontal advection**

201 The low-salinity chlorophyll-rich water originating from the northern coastal region often accompanying
202 heavy rainfalls is advected equatorward along the coast into the coastal zone in the vicinity of the ESROB in
203 summer, and is primarily responsible for most (80 %) of the CF events. The rate of Chl a change observed at
204 the ESROB is comparable with the rate estimated from the spatial Chl a gradient and speed of equatorward
205 advection. The equatorward advection distance of high Chl a water is measured to 100 km (= dy) over 3 days
206 (= dt) with Chl a change of about 2.5 µg/l (= dChl) from the series of four daily composites of satellite-
207 measured Chl a collected in July 24 to 27, 2013 before E09 (Fig. 9a, b, c and d). With an advective speed of
208 0.4 m/s (= 100 km / 3 days), this yields a rate of Chl a change of 0.86 µg/l d⁻¹ (= 0.4 m/s × 2.5 µg/l / 100 km)
209 owing to the alongshore advection ($v\partial\text{Chl } a/\partial y$), which is consistent with the observed rate ($\partial\text{Chl } a/\partial t$)
210 where dChl was estimated from the ESROB measurements and dt = 1 h) for E09 (up to 1.26 µg/l d⁻¹ averaged
211 over the period when $\partial\text{Chl } a/\partial t > 0$) and others (mean: 0.87 µg/l d⁻¹), supporting that the alongshore
212 advection plays a primary role in CF variability near the coast. These findings are similar to those of bloom
213 events with a rate of CF change (2–4 µg/l d⁻¹ estimated from their Fig. 11) controlled by the advection of low
214 SSS and high CF plume water in other coastal systems (Halverson and Pawlowicz, 2013).

215 In contrast to E09, the high surface CF observed during E07 is not explained by equatorward advection of



216 low-salinity chlorophyll-rich water originating from the northern coastal region, but potentially by the
217 onshore advection of high CF water of southern origin advected via the EKWC. Hyun et al. (2009)
218 demonstrated that the highest primary productivity in the southwestern East Sea is induced by the
219 transportation of high CF water originated from upwelling of nutrient rich water along the southern east coast
220 of Korea. The high CF water may affect the productivity near the mid-east coast of Korea as advected by the
221 EKWC and its meanders, particularly on the western or coastal side of the front formed by the EKWC. Indeed,
222 a rate of cross-shore Chl *a* change around ESROB from the surface CF distribution observed during E07 (Fig.
223 9a) is roughly $0.1 \mu\text{g/l km}^{-1}$ ($\text{dChl } a = 1.0 \mu\text{g/l}$ and $\text{dx} = 10 \text{ km}$) and a rate of Chl *a* change by cross-shore
224 advection ($u \partial \text{Chl } a / \partial x$) is estimated to $0.86 \mu\text{g/l d}^{-1}$ ($= 0.1 \text{ m/s} * 1.0 \mu\text{g/l} / 10 \text{ km}$) with cross-shore velocity
225 of 0.1 m/s (estimated from the ESROB measurements), which supports this assertion, demonstrating a high
226 CF region offshore of ESROB (Fig. 9a, d). Onshore advection of the high CF water originated from the
227 upwelling of nutrient rich water along the coast, accounting for half the CF change during the event (up to
228 $1.60 \mu\text{g/l d}^{-1}$ averaged over the E07 when $\partial \text{Chl } a / \partial t > 0$) observed at ESROB during E07 (Fig. 7).
229 Conversely, offshore advection of high CF coastal plume water of northern origin may also be significant as
230 that of E10. Based on previous research conducted in other coastal systems, E10 is similar to results on
231 temporal and spatial variations of CDOM, CF, and primary productivity by cross-shore (onshore and/or
232 offshore) advection of high SST and high CF plume water associated with local circulations (Brzezinski and
233 Washburn, 2011; Warrick et al., 2007). Thus, cross-shore advection of low SSS and high CF water associated
234 with ambient circulation plays an equally significant role in shaping and triggering bloom events in the
235 coastal area.

236

237 **4.2. Other mechanisms**

238 The high CF events observed at ESROB are not local blooms triggered by either nutrients or light
239 availability. The upward vertical flux of nitrate into the euphotic zone at Huntington Beach, southern
240 California shows how vertical nutrient supply triggers local chlorophyll blooms (Omand et al., 2012). Omand
241 et al. (2012) demonstrated that each episodic bloom was preceded by a vertical nitrate flux event 6–10 days
242 earlier using nitrate concentrations estimated from a temperature proxy. Relationships between nitrate and
243 temperature and between nitrate and salinity observed from the surveys in July and October of 2011 and
244 April of 2012 are not significantly different each other, and the vertical nitrate fluxes were estimated by the
245 temperature proxy to discuss the potential role of nitrate in triggering the episodic blooms. However, both
246 advective and turbulent nitrate fluxes estimated using a nitrate proxy utilized from temperature
247 measurements (Fig. 10) did not account for the observed CF blooms (not shown). Although some episodic
248 CF blooms (E01 and E06) are preceded by flux peaks with a typical time lag of 4–12 d, most events are not
249 directly linked to the variability in vertical nitrate fluxes, suggesting only minor roles of nutrient flux in
250 shaping CF variability observed at ESROB in summer.

251 Time-series of the euphotic zone (Z_{eu}) was compared with others to examine the effects of light adaptation
252 on the bloom events from two PAR sensors available for 2012 and 2013 (Figs. 6, 7). Basically, Z_{eu} of 18 m



253 averaged over E04–E10 was deeper than 10.5 m which is Z_{eu} averaged over the two whole summer periods
254 (JJAS), indicating that the light environment was favorable at least for retaining and increasing of the CF
255 bloom observed at ESROB. Z_{eu} of 20 m averaged over the three bloom events (E04–E06) in 2012 was deeper
256 than that ($Z_{eu}=15$ m for E07–E10) in 2013, supporting more favorable CF bloom conditions in 2012 than
257 2013. Correspondingly, CF of 1.8 $\mu\text{g/l}$ averaged over E04–E06 in 2012 was higher than that in 2013 (~ 1.6
258 $\mu\text{g/l}$ for E07–E10). Our results on the deeper Z_{eu} with higher CF in 2012 than 2013 summers are consistent
259 with those in other systems (e.g., Mississippi River coastal system) where light attenuation plays a significant
260 role in increasing phytoplankton biomass, and productivity variation (Lehrter et al., 2009). However, the CF
261 changes among the individual events do not necessarily follow Z_{eu} variations (Table 1), suggesting a minor
262 role of light availability in shaping the CF variability observed at ESROB.

263

264 **4.3. Inter-annual variations**

265 The CF bloom events near the coast can vary inter-annually depending on the passage of typhoons. Five
266 typhoons passed through this area were associated with the CF bloom events for two summers (2011 and
267 2012) and there was no typhoon affecting the CF bloom events in 2013 summer. Both strong wind forcing
268 and intensive rainfalls associated with typhoon passage nearby determine how the plume water is advected
269 in and around ESROB, which varies year-to-year. In 2011, for example, the CF enhancement (E01) was
270 accompanied by the passage of MAON (equatorward wind stress and current) through the area south of
271 ESROB, whereas E03 ended with the passage of MUIFA (poleward wind stress and current) passing through
272 the area north of ESROB (Fig. 5b). Similarly, surface CF decreased (increased) with the passages of typhoons
273 KHANUN and BOLAVEN (TENBIIN) through the area north (south) of ESROB (Fig. 6b). Without any
274 typhoon passage in the summer of 2013, only half the CF events could be explained by the alongshore
275 advection contrasting with those in the other two years (Fig. 7b). Thus, the primary productivity in the area
276 is possibly affected severely by inter-annual variations of typhoon-induced alongshore advection.

277 Remote wind forcing significantly affecting summer-time equatorward currents near the coast via
278 equatorward propagating coastal trapped waves (CTWs) varied in the summers of 2011, 2012, and 2013
279 (Park et al., 2018 submitted). The CTWs generated off the Russian coast (~1,000 km from ESROB) changed
280 equatorward currents at the location of ESROB to yield more equatorward advection in 2011 and 2012
281 summers and more poleward advection in 2013 summer, of low-salinity plume water near the coast (Park et
282 al., 2018 submitted). These results may be relevant to more CF bloom events explained by equatorward
283 advection of plume water of northern origin in 2011 and 2012 summers than 2013 summer (6 among 6 events
284 vs. 2 among 4 events). Therefore, inter-annual variations of alongshore advection and surface CF blooms
285 near the coast are possibly affected the CTWs propagating equatorward from the Russian coast, where wind
286 forcing varies considerably to generate CTWs. Park et al. (2018 submitted) also quantified the impact of
287 EKWC on the alongshore current variability near the coast, which yields less EKWC impact and more
288 equatorward currents near the coast in 2011 and 2013 summers, than 2012 summer. Although this is
289 inconsistent with less CF bloom events explained by the equatorward advection of plume water of northern



290 origin in 2013 summer, cross-shore advections of high CF water of either northern (E10) or southern origin
291 (E07) are possibly associated with EKWC recirculation based on the patterns of surface geostrophic currents
292 (Fig. 9).

293

294 **5. Concluding remarks**

295 The low-salinity chlorophyll-rich water originating from the northern coast accompanying heavy rainfalls is
296 often advected equatorward along the coast in summer, resulting in high surface CF enhancements near the
297 mid-east coast of Korea. Alongshore advection of high CF waters is primarily responsible for most (80 %, 8
298 of 10) of the CF events, which confirms that the bloom events are possibly controlled by the advection of
299 low SSS and high CF plume water in summer. In contrast to the bloom events associated with alongshore
300 advection, the high surface CF observed during E07 is possibly explained by the onshore advection of high
301 CF water of southern origin advected by the poleward-flowing EKWC. Similarly, offshore advection of high
302 CF coastal plume water of northern origin may be significant, as in the case of E10. Therefore, the
303 equatorward and cross-shore advections of chlorophyll-rich plume water with decreasing SSS plays a
304 primary role in the high productivity near the east coast of Korea in summer. Summer-time CF near the coast
305 varies inter-annually as the horizontal advections vary significantly, inter-annually associated with typhoon
306 passages nearby, CTWs generated from the Russian coast, and influence of the EKWC, which should be
307 addressed with long time series data in future.

308

309 **Acknowledgements**

310 We thank Kyung-Il Chang for his helpful comments to improve the original version of this paper.
311 Geostationary ocean color satellite data (chlorophyll and total suspended sediment), precipitation (rain), and
312 satellite altimetry-derived sea surface height data were provided by the KIOST (Korea Institute Ocean
313 Science and Technology), KMA (Korea Meteorological Administration), and AVISO (Archiving, Validation,
314 and Interpretation of Satellite Oceanographic data), respectively. This research was supported by the Basic
315 Science Research Program through the National Research Foundation of Korea (NRF) funded by the
316 Ministry of Education (No. 2017R1D1A1B03035958 and NRF-2015R1D1A1A02062252), and was a part
317 of the project titled “Deep Water Circulation and Material Cycling in the East Sea”, funded by the Ministry
318 of Oceans and Fisheries, Korea. This work is partly supported by the Agency for Defense Development
319 (UD170006DD), Korea.

320

321 **Data availability:** All data are available upon request to the authors.

322 **Author contributions:** This work was conceptualized and funding was secured by SHN and YTS. In-situ
323 measurements were designed by SHN and YTS, and performed by YTS and JHP with equipment provided



324 by SHN and YTS. Data were analyzed by YTS and JHP. The manuscript was written by YTS and SHN and
325 edited by YTS, SHN, and JHP. All authors have approved the final article.

326 **Competing interests:** The authors declare that they have no conflict of interest.

327

328 **References**

- 329 Bae, D. H., Jung, I. W., and Chang, H.: Long-term trend of precipitation and runoff in Korean river basins, *Hydro.
330 Proc.*, 22, 2644-2656, 10.1002/hyp.6861, 2008.
- 331 Brzezinski, M. A., and Washburn, L.: Phytoplankton primary productivity in the Santa Barbara Channel: Effects
332 of wind-driven upwelling and mesoscale eddies, *J. Geophys. Res.*, 116, 10.1029/2011jc007397, 2011.
- 333 Choi, B.-J., Byun, D.-S., and Lee, K.-H.: Satellite-altimeter-derived East Sea surface currents: Estimation,
334 description and variability pattern, *The Sea*, 17, 225-242, 10.7850/jkso.2012.17.4.225, 2012.
- 335 Crespo, B. G., Figueiras, F. G., and Groom, S.: Role of across-shelf currents in the dynamics of harmful
336 dinoflagellate blooms in the northwestern Iberian upwelling, *Limnol. Oceanogr.*, 52, 2668-2678, DOI
337 10.4319/lo.2007.52.6.2668, 2007.
- 338 Dai, M. H., Zhai, W. D., Cai, W. J., Callahan, J., Huang, B. Q., Shang, S. L., Huang, T., Li, X. L., Lu, Z. M., Chen,
339 W. F., and Chen, Z. Z.: Effects of an estuarine plume-associated bloom on the carbonate system in the lower
340 reaches of the Pearl River estuary and the coastal zone of the northern South China Sea, *Cont. Shelf Res.*, 28,
341 1416-1423, 10.1016/j.csr.2007.04.018, 2008.
- 342 Halverson, M. J., and Pawlowicz, R.: High-resolution observations of chlorophyll-a biomass from an instrumented
343 ferry: Influence of the Fraser River plume from 2003 to 2006, *Cont. Shelf Res.*, 59, 52-64,
344 10.1016/j.csr.2013.04.010, 2013.
- 345 Hong, G. H., Lee, D. K., Yang, D. B., Kim, Y. I., Park, J. H., and Park, C. H.: Eddy- and wind-sustained moderate
346 primary productivity in the temperate East Sea (Sea of Japan), *Biogeosci. Disc.*, 10, 10429-10458,
347 10.5194/bgd-10-10429-2013, 2013.
- 348 Hyun, J., Kim, D., Shin, C., Noh, J., Yang, E., Mok, J., Kim, S., Kim, H., and Yoo, S.: Enhanced phytoplankton
349 and bacterioplankton production coupled to coastal upwelling and an anticyclonic eddy in the Ulleung basin,
350 East Sea, *Aquat. Microbial Ecol.*, 54, 45-54, 10.3354/ame01280, 2008.
- 351 Kang, J. H., Kim, W. S., Chang, K. I., and Noh, J. H.: Distribution of plankton related to the mesoscale physical
352 structure within the surface mixed layer in the southwestern East Sea, Korea, *J. Plankton Res.*, 26, 1515-1528,
353 10.1093/plankt/fbh140, 2004.
- 354 Kim, D., Yang, E. J., Kim, K. H., Shin, C. W., Park, J., Yoo, S., and Hyun, J. H.: Impact of an anticyclonic eddy
355 on the summer nutrient and chlorophyll a distributions in the Ulleung Basin, East Sea (Japan Sea), *ICES J.
356 Mar. Sci.*, 69, 23-29, 10.1093/icesjms/fsr178, 2011.
- 357 Kong, G. S., Kim, K.-O., and Kim, S.-P.: Characteristics of the East Asian summer monsoon in the South Sea of
358 Korea during the Little Ice Age, *Quaternary International*, 286, 36-44, 10.1016/j.quaint.2012.07.022, 2013.
- 359 Lehrter, J. C., Murrell, M. C., and Kurtz, J. C.: Interactions between freshwater input, light, and phytoplankton
360 dynamics on the Louisiana continental shelf, *Cont. Shelf Res.*, 29, 1861-1872, 10.1016/j.csr.2009.07.001,
361 2009.
- 362 Müller, P., Li, X., and Niyogi, K. K.: Non-Photochemical Quenching. A Response to Excess Light Energy, *Plant
363 Physiol.*, 125, 1558-1566, <http://doi.org/10.1104/pp.125.4.1558>, 2001.
- 364 Nam, S., Kim, G., Kim, K.-R., and Kim, K.: Application of Real-time Monitoring Buoy Systems for Physical and
365 Biogeochemical Parameters in the Coastal Ocean around the Korean Peninsula, *Mar. Technol. Soc. J.*, 39, 70-
366 80, 2005.
- 367 Omand, M. M., Feddersen, F., Guza, R. T., and Franks, P. J. S.: Episodic vertical nutrient fluxes and nearshore
368 phytoplankton blooms in Southern California, *Limnol. Oceanogr.*, 57, 1673-1688, 10.4319/lo.2012.57.6.1673,
369 2012.
- 370 Park, J.-H., Chang, K.-I., and Nam, S.: Summertime coastal current reversal opposing offshore forcing and local
371 wind near the middle east coast of Korea: Observation and dynamics, *Geophys. Res. Lett.*, 43, 7097-7105,
372 10.1002/2016gl069322, 2016.
- 373 Park, J.-H. and Nam, S.: Interannual variability of a surface alongshore current near the mid- latitude western
374 boundary: A summer case on the Korean east coast, *Journal of Geophysical Research: Oceans* (submitted).
- 375 Reifel, K. M., Corcoran, A. A., Cash, C., Shipe, R., and Jones, B. H.: Effects of a surfacing effluent plume on a



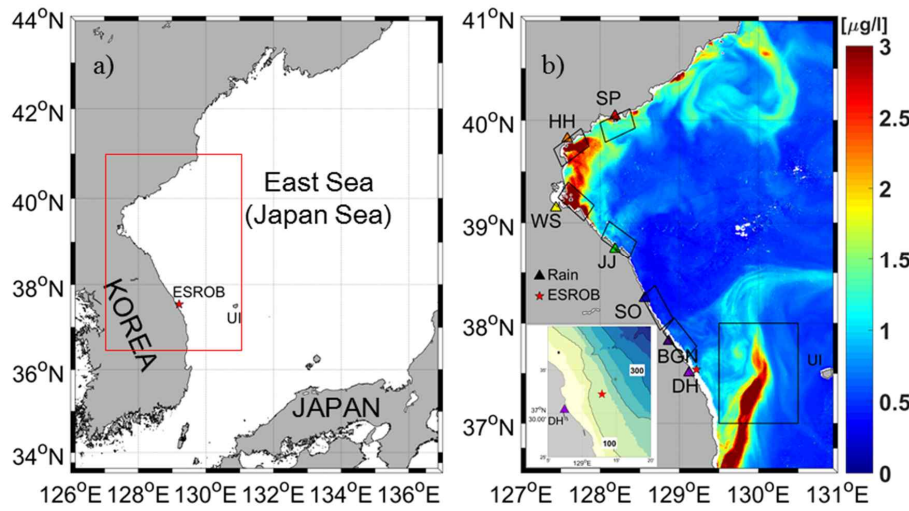
- 376 coastal phytoplankton community, *Cont. Shelf Res.*, 60, 38-50, 10.1016/j.csr.2013.04.012, 2013.
377 Ryu, J.-H., Han, H.-J., Cho, S., Park, Y.-J., and Ahn, Y.-H.: Overview of geostationary ocean color imager (GOCI)
378 and GOCI data processing system (GDPS), *Ocean Sci. J.*, 47, 223-233, 10.1007/s12601-012-0024-4, 2012.
379 Son, Y. T., Chang, K. I., Yoon, S. T., Rho, T., Kwak, J. H., Kang, C. K., and Kim, K. R.: A newly observed physical
380 cause of the onset of the subsurface spring phytoplankton bloom in the southwestern East Sea/Sea of Japan,
381 *Biogeosci.*, 11, 1319-1329, 10.5194/bg-11-1319-2014, 2014.
382 Warrick, J. A., DiGiocomo, P. M., Weisberg, S. B., Nezlin, N. P., Mengel, M., Jones, B. H., Ohlmann, J. C.,
383 Washburn, L., Terrill, E. J., and Farnsworth, K. L.: River plume patterns and dynamics within the Southern
384 California Bight, *Cont. Shelf Res.*, 27, 2427-2448, 10.1016/j.csr.2007.06.015, 2007.
385 Yin, K. D., Zhang, J. L., Qian, P. Y., Jian, W. J., Huang, L. M., Chen, J. F., and Wu, M. C. S.: Effect of wind events
386 on phytoplankton blooms in the Pearl River estuary during summer, *Cont. Shelf Res.*, 24, 1909-1923,
387 10.1016/j.csr.2004.06.015, 2004.
388 Yoo, S., and Kim, H. C.: Suppression and enhancement of the spring bloom in the southwestern East Sea/Japan
389 Sea, *Deep-Sea Res. Pt. II*, 51, 1093-1111, 10.1016/j.dsr2.2003.10.008, 2004.
390
- 391
392
- 393



394 Table 1. Sea surface temperature (SST) in °C, sea surface salinity (SSS) in g/kg, chlorophyll-a fluorescence (CF)
395 in µg/l, duration in day, and euphotic depth (Z_{eu}) in m during the E01–E10 observed from the surface mooring
396

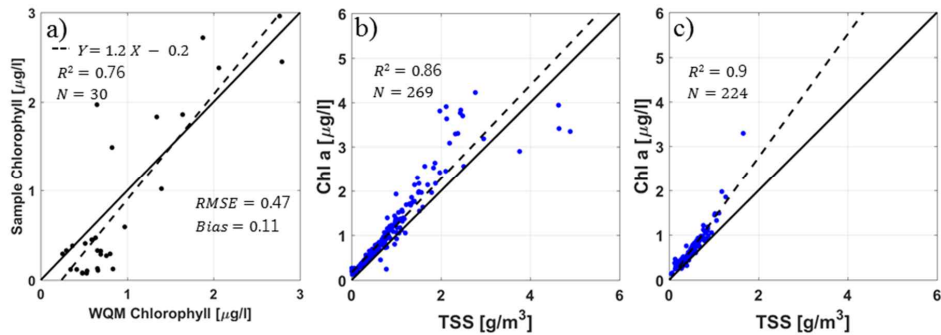
397

		SST	SSS	CF (start & end dates)	Duration	Z_{eu}
2011	E01	20.5	31.2	1.65 (21. Jul. ~ 25. Jul.)	4.9	Not available
	E02	22.3	30.9	1.91 (26. Jul. ~ 03. Aug.)	8.3	Not available
	E03	24.3	29.9	1.61 (05. Aug. ~ 08. Aug.)	2.5	Not available
	E04	21.4	32.9	1.67 (16. Jul. ~ 20. Jul.)	3.5	22
	E05	22.8	32.8	1.29 (21. Jul. ~ 27. Jul.)	5.8	20.6
	E06	18.1	33.4	2.35 (29. Aug. ~ 05. Sep.)	6.4	16.8
	E07	16.1	34.1	1.6 (01. Jul. ~ 04. Jul.)	2.3	17.8
	E08	21.2	33.2	1.6 (12. Jul. ~ 16. Jul.)	4.4	15.7
	E09	25.0	32.1	1.7 (28. Jul. ~ 01. Aug.)	4.3	12.7
	E10	26.7	31.9	1.4 (18. Aug. ~ 23. Aug.)	5.9	15.2



398
399

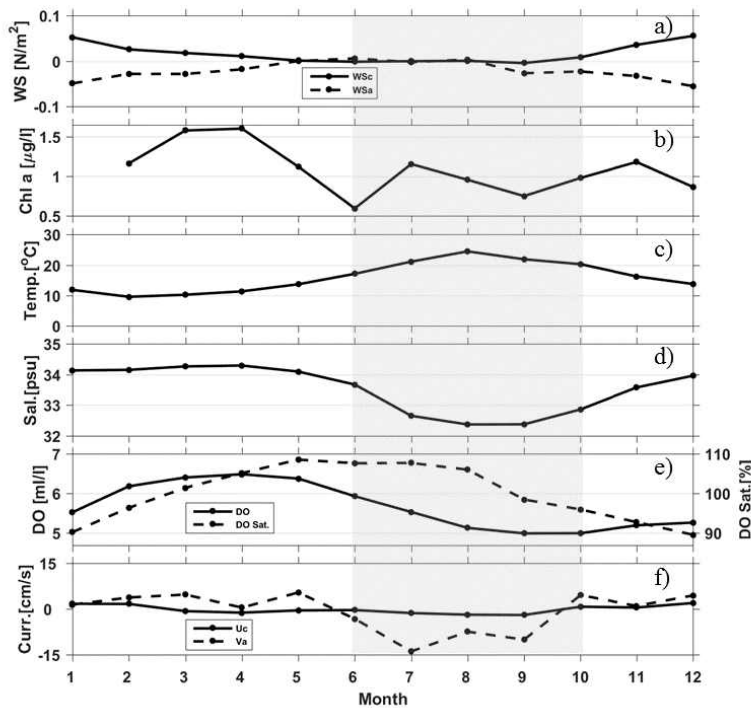
400 Figure 1. a) Study area in the western part of the East Sea (Japan Sea). b) A chlorophyll a image from
401 the geostationary ocean color satellite on September 6, 2012 in the area marked by red box in a). Black solid boxes
402 denote the areas where the chlorophyll a and TSS are averaged. Locations of the rainfall station along the east
403 coast of Korea are marked by triangles (SP: SinPho, HH: HamHeung, WS: WonSan, JJ: JangJun, SO: Sockcho,
404 BGN: BukGangNeung, DH: DongHae, rainbow colored). The surface mooring (ESROB) is indicated by a red
405 star in b) with bottom topography in the lower left corner where numbers denote water depth in meter (contour
406 interval: 100 m). Ulleung Island (UI) is located at ~ 131 °E.
407



408

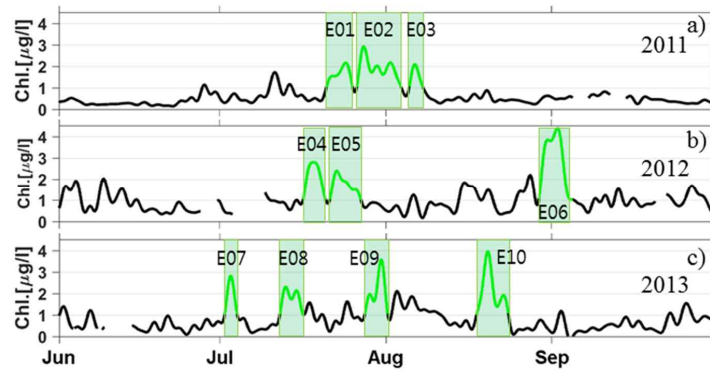
409 Figure 2. Results of cross-correlation (R^2 : correlation coefficient) and linear regression analyses (dash lines)
410 between a) chlorophyll fluorescence measured by the ESROB WQM and absolute chlorophyll concentration
411 obtained from in-situ water samples; and between TSS and chlorophyll a concentration for b) the areas along and
412 near the east coast of Korea and c) area off the coast between DH and UI. The water samples (N: sample number)
413 were collected in July and October of 2011 and April of 2012.

414



415

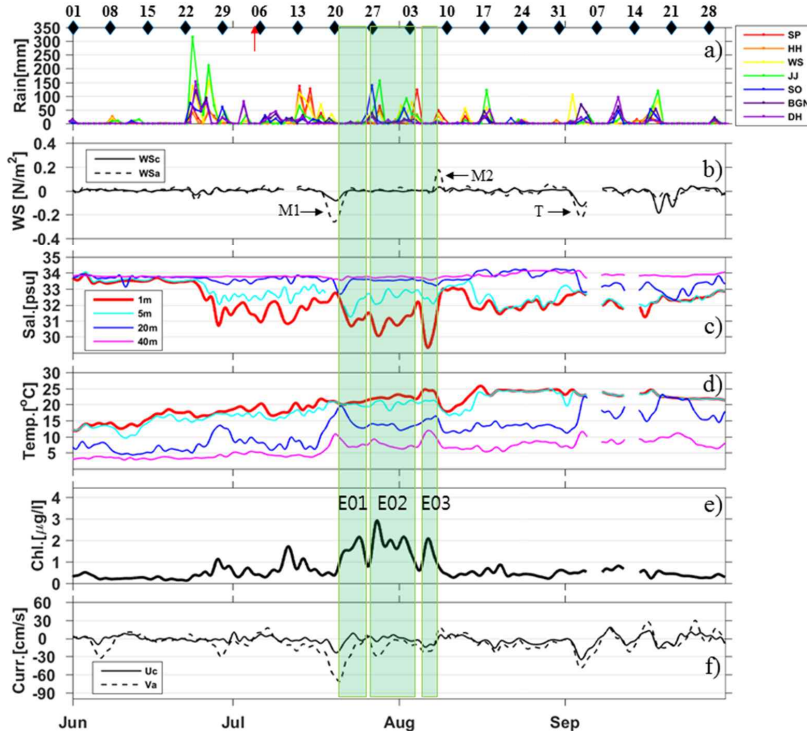
416 Figure 3. Climatology for a) alongshore and cross-shore components of wind stress,
417 b) chlorophyll fluorescence,
418 c) water temperature,
419 d) salinity,
420 e) dissolved oxygen in both ml/l and percentage saturation, and f) alongshore
421 and cross-shore components of surface (~ 5 m) current constructed using ESROB data collected in three years
from 2011 to 2013. Summer season (JJAS) is shaded.



421

422 Figure 4. Time-series of low-pass filtered (cutoff period of 40 h) chlorophyll fluorescence observed at the ESROB
423 during the three summers (JJAS) of a) 2011, b) 2012, and c) 2013. The episodic bloom events are green-shaded
424 and labeled E01 to E10.

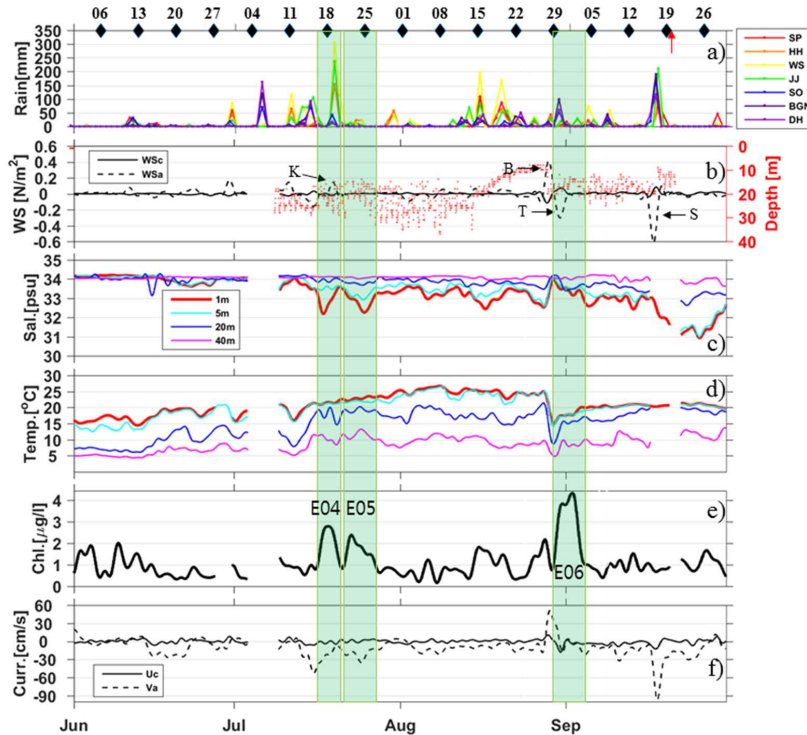
425



426

427 Figure 5. Time-series data collected in 2011 of a) daily rainfall amounts observed at weather stations (SP: SinPho,
 428 HH: HamHeung, WS: WonSan, JJ: JangJun, SO: Sockcho, BGN: BukGangNeung, DH: DongHae) along the east
 429 coast of Korea, and b) alongshore (solid) and cross-shore (dash) wind stresses, c) salinities, and d) water
 430 temperatures observed at surface (red), 5 (cyan), 20 (blue), and 40 m (pink), e) surface CF, and f) alongshore
 431 (dashed) and cross-shore (solid) currents, observed at the ESROB. The bloom events are labeled by E01 to E03.
 432 In the top axis of (a), dates/times of satellite altimetry-derived surface geostrophic current map and geostationary
 433 satellite ocean color image are remarked with black diamonds and red arrow, respectively. Nearby passages of
 434 typhoons are indicated by black arrows in b) (M1: MAON, M2: MUIFA and T: TALAS).

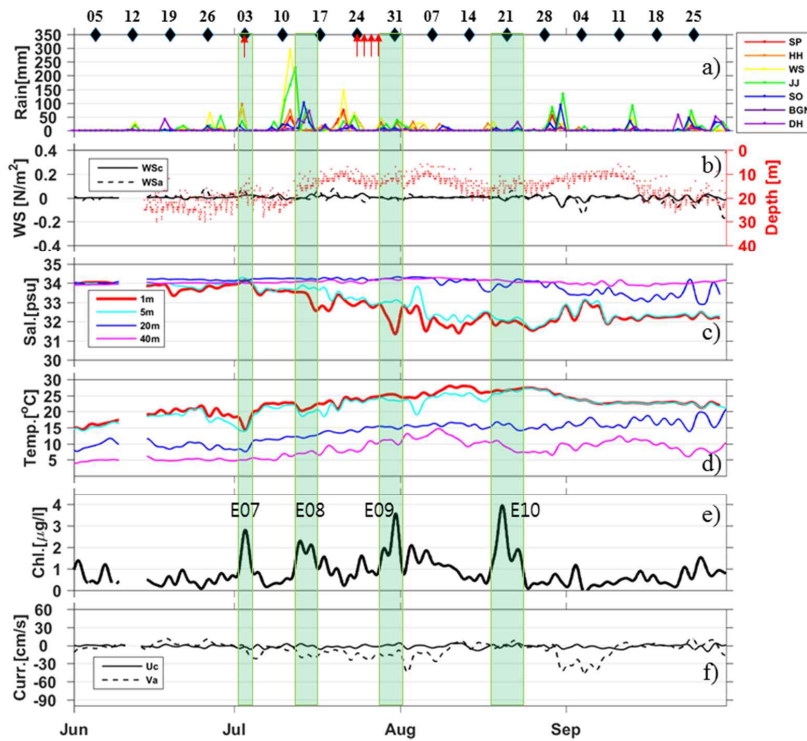
435



436

437 Figure 6. Same as Figure 5, except for 2012 bloom events labeled E04 to E06,
 438 and four typhoons (K: KHANUN,
 439 T: TENBIN, B: BOLAVEN, S: SANBA). Euphotic depth (Z_{eu} , red dots) derived from two PAR sensors attached
 to the ESROB are superimposed in b).

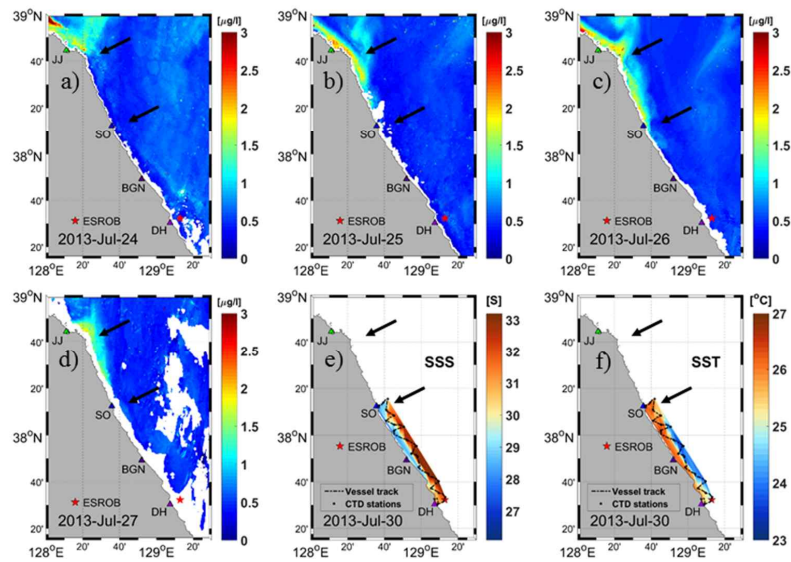
440



441

442 Figure 7. Same as Figure 6 except for 2013 bloom events labeled E07 to E10, and no typhoon occurrence.

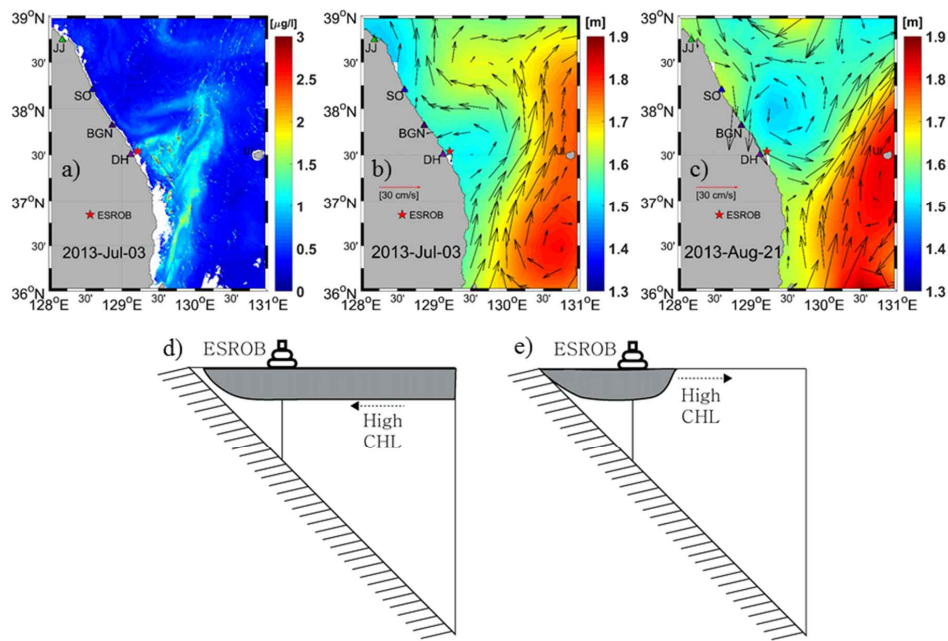
443



444

445 Figure 8. a)-d) Daily series of geostationary satellite ocean color images indicating surface chlorophyll a
446 distributions from July 24 to 27, 2013. Surface distributions of e) salinity and f) temperature observed using a
447 small research vessel (ship tracks and CTD stations are remarked with dashed lines and dots) in July 30, 2013 a
448 couple of days after heavy rainfall in the region. Two black arrows in each panel head for the same locations in
449 the vicinity of JJ (JangJun) and SO (Sockcho).

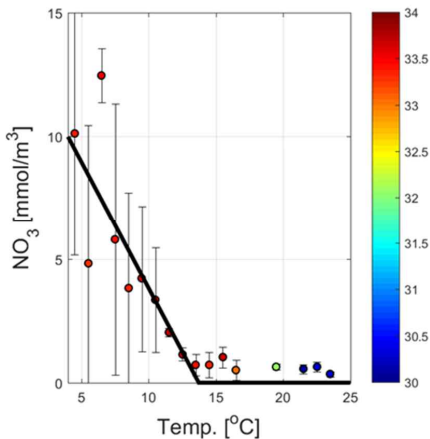
450



451

452 Figure 9. Distributions of a) daily composite of chlorophyll a concentration in July 3, 2013, obtained from the
453 geostationary satellite ocean color imager, and satellite altimetry-derived surface geostrophic currents in b) July
454 3 and c) August 21, 2013. Schematics for (d) on-shore and (e) off-shore advectons of high CF surface water for
455 July 3 (E07) and August 21 (E10), 2013.

456



457

458 Figure 10. A linear fit (bold line) between temperature (Temp.) and nitrate (NO_3) for Temp. < 14.0 °C ($\text{NO}_3 = 0$ for
459 Temp. > 14.0 °C) to observations near the east coast of Korea in summers of 2011 and 2012. A standard deviation
460 of nitrate and absolute salinity in g/kg are shown with vertical bars and colors (colorbar in the right), respectively.

461